

# Differential freezeout and pion interferometry at RHIC from covariant transport theory

Dénes Molnár<sup>1,2</sup> and Miklos Gyulassy<sup>2</sup>

<sup>1</sup>*Department of Physics, Ohio State University, 174 West 18th Ave, Columbus, OH 43210*

<sup>2</sup>*Department of Physics, Columbia University, 538 West 120-th Street, New York, NY 10027*

(Dated: November 3, 2018)

Puzzling discrepancies between recent pion interferometry data on  $Au+Au$  reactions at  $\sqrt{s} = 130$  and 200 AGeV from RHIC and predictions based on ideal hydrodynamics are analyzed in terms of covariant parton transport theory. The discrepancies of out and longitudinal radii are significantly reduced when the finite opacity of the gluon plasma is taken into account.

PACS numbers: 12.38.Mh; 24.85.+p; 25.75.Gz; 25.75.-q

*Introduction.* Decoupling, or freezeout of final state interactions, is a process with unique sensitivity to the space time evolution of hadronic interactions. It reflects the interplay between the decreasing opacity of the system at late times and correlations induced by collective expansion driven by high scattering rates at early times.

In heavy-ion physics, information about the spacetime decoupling geometry can be obtained via identical boson (Hanbury-Brown and Twiss (HBT)) interferometry. Recent two pion correlation data in Au+Au at  $\sqrt{s} = 130$  [1, 2] and 200 AGeV/nucleon [3] at RHIC seem at first sight to indicate a sudden freezeout that is difficult to reconcile with the strong collective dynamics implied by the substantial elliptic flow  $v_2 \sim 0.1$  also observed [4, 5].

Ideal Euler hydrodynamics provides one of the powerful covariant approaches to predict the collective flow pattern as well as possible freezeout hypersurfaces in heavy-ion collisions. However, this approach predicts an "out" radius,  $R_{out}$  as defined below, significantly larger than the "side" radius,  $R_{side}$  [6, 7]. On the other hand, it is possible that the failure of non-dissipative hydrodynamics to correctly describe the delicate space-time decoupling geometry is due to the neglect of deviations from local equilibrium throughout the evolution. HBT predictions with hydrodynamics are based on an additional ad hoc (Cooper-Frye) postulate that freezeout occurs on some "thin" three-dimensional hypersurface (typically, an isotherm). Only a detailed covariant transport theory can assess the theoretical error introduced by this postulate.

The simplest Lorentz covariant dynamical framework that can predict freezeout *self-consistently* is transport theory [8, 9, 10, 11]. In this approach the interaction rate is controlled by microscopic differential cross sections,  $d\sigma$ . As the system expands and rarefies, the scattering rate decreases until the particles stop interacting. In [8] it was emphasized that finite cross sections are needed to account for the saturation of differential elliptic flow  $v_2(p_\perp)$  observed for  $p_\perp > 2$  GeV in Au+Au at RHIC [4, 5].

The influence of final state dissipation on HBT was studied in a hybrid hydrodynamic/transport model in Ref. [12]. In that work, hydrodynamical evolution was followed only up to a hadronization isotherm  $T(x^\mu) = T_c$ .

Subsequently, the decoupling of the hadron gas was computed via the UrQMD hadronic transport model. However, the predicted  $R_{out}/R_{side} > 1$  increasing with transverse momentum still fails to account for the observed decreasing  $R_{out}/R_{side} < 1$ . Similar hadronic transport results were reported in [13]. This suggests that possible deviations from the local equilibrium assumption prior to hadronization should also be explored.

Recently, a combined parton/hadron transport theory approach was proposed in [14]. The results suggest that the HBT radii are indeed sensitive to the parton cross section during the dense partonic phase of the reaction. Unfortunately, all the transport calculations above left open the delicate question of Lorentz covariance of the numerical solutions. In any case, we note that no transport or hydrodynamic calculation has as yet been able to reproduce the phenomenological decoupling source parametrizations fitted to that data in [15].

In this letter, we concentrate exclusively on the partonic transport phase to isolate more clearly the influence of dissipative partonic processes on the decoupling geometry and study in detail the question of covariance. Preliminary results were reported in [16]. We utilize the MPC numerical technique [17], and compute the covariant freezeout distributions for a wide range of RHIC initial conditions as a function of the partonic opacity.

*Two-particle HBT interferometry.* For a chaotic boson freeze-out source  $\rho(\vec{x}, t)$ , the two-particle momentum correlation function  $C(p_1, p_2)$  is given by the *space-time* Fourier transform of the source [18, 19, 20]. Although the relation cannot be inverted (due to loss of phase information and the on mass-shell constraint), HBT measurements provide a unique test of freezeout distributions and dynamical scenarios in heavy-ion collisions.

Conventionally, the two-particle correlation function is expressed in terms of the relative momentum  $q^\mu \equiv p_1^\mu - p_2^\mu$  and average pair momentum  $K^\mu \equiv (p_1^\mu + p_2^\mu)/2$ . The 'out-side-long' variables,  $q_O$ ,  $q_S$ , and  $q_L$ , are then defined via  $\vec{q}_{LCMS} \equiv (q_O, q_S, q_L)$  in the Longitudinal Center of Mass System (LCMS) reference frame where  $K_{LCMS}^\mu = (\vec{K}^0, K_\perp, 0, 0)$ . We denote here the LCMS spacetime coordinates by  $x_{LCMS}^\mu \equiv (\tilde{t}, x_O, x_S, x_L)$ .

Experimentally, the measured correlation function (af-

ter correcting for Coulomb distortions) is fitted with a Gaussian, which for central collisions and at midrapidity is constrained by symmetry to the form

$$C(\vec{q}, K) = 1 + \lambda(K) \exp \left[ - \sum_{i=O,S,L} q_i^2 R_i^2(K) \right]. \quad (1)$$

Here  $R_O$ ,  $R_S$  and  $R_L$  are the 'out', 'side', and 'long' HBT radii. For a *perfectly Gaussian* source, the correlation function is Gaussian and [20]

$$\begin{aligned} R_O^2(K) &= \langle \Delta x_O^2 \rangle_K + v_\perp^2 \langle \Delta \tilde{t}^2 \rangle_K - 2v_\perp \langle \Delta x_O \Delta \tilde{t} \rangle_K \\ R_S^2(K) &= \langle \Delta x_S^2 \rangle_K, \quad \text{and} \quad R_L^2(K) = \langle \Delta x_L^2 \rangle_K, \end{aligned} \quad (2)$$

where  $v_\perp \equiv K_\perp / \tilde{K}^0$ . Thus  $R_S$  and  $R_L$  have simple geometric interpretation as the 'side' and 'long' widths of the distribution function, while  $R_O$  is a mixture of the 'out' width, time spread, and the  $x_O - \tilde{t}$  correlation.

*Covariant parton transport theory.* We consider here, as in Refs. [8, 9, 10], the simplest but nonlinear form of Lorentz-covariant Boltzmann transport theory in which the on-shell phase space density  $f(x, \vec{p})$ , evolves with an elastic  $2 \rightarrow 2$  rate as

$$\begin{aligned} p_1^\mu \partial_\mu \tilde{f}_1 &= \tilde{S}(x, \vec{p}_1) + \frac{\pi^4}{2} \iiint_{234} (\tilde{f}_3 \tilde{f}_4 - \tilde{f}_1 \tilde{f}_2) |\overline{\mathcal{M}}_{12 \rightarrow 34}|^2 \\ &\quad \times \delta^4(p_1 + p_2 - p_3 - p_4). \end{aligned} \quad (3)$$

Here  $|\overline{\mathcal{M}}|^2$  is the polarization averaged scattering matrix element squared, the integrals are shorthands for  $\int_i \equiv \int d^3 p_i / [(2\pi)^3 E_i]$ , while  $f_j \equiv (2\pi)^3 f(x, \vec{p}_j)$ . The initial conditions are specified by the source function  $\tilde{S}(x, \vec{p})$ . For our applications below, we neglect quark degrees of freedom and interpret  $f(x, \vec{p})$  as describing an ultrarelativistic massless gluon gas (8 colors, 2 helicities).

Eq. (3) can be extended to include inelastic matrix elements, such as  $gg \leftrightarrow ggg$ , and proper Bose or Fermi statistics can be introduced as well. However, at present there is no *practical* algorithm to compute accurate numerical solutions to such transport equations on the workstations available to us. Therefore, the present study is limited to the classical case with elastic  $2 \rightarrow 2$  interactions.

The elastic gluon scattering matrix elements in dense parton systems were modeled with the isotropic form  $d\sigma_{el}/dt = \sigma_0(s)/s$ , as justified by our previous study[8]. We showed in [8] that the covariant transport solutions do not depend *explicitly* on the differential cross section but only on the *transport opacity*

$$\chi \equiv \frac{\sigma_{tr}}{\sigma_{el}} \langle n \rangle \approx \sigma_{tr} \langle \int dz \rho(\mathbf{x}_0 + z \hat{\mathbf{n}}, \tau = \frac{z}{c}) \rangle, \quad (4)$$

where  $\sigma_{tr}(s) \equiv \int d\sigma_{el} \sin^2 \theta_{cm}$  is the transport cross section (in our case,  $\sigma_{tr} = 2\sigma_0/3$ ), and  $\langle n \rangle$  is the average number of scatterings per parton. For a fixed nuclear geometry, a given transport opacity  $\chi$  represents a *whole*

*class* of initial conditions and partonic matrix elements, as demonstrated by the approximate proportionality[8]  $\chi \propto \sigma_{tr} dN_g(\tau_0)/d\eta$ .

We solved Eq. (3) numerically via the MPC parton cascade algorithm[17]. MPC utilizes the particle subdivision technique[9], which is essential to eliminate numerical artifacts caused by frame-dependent collision ordering and acausal (superluminal) propagation due to action at a distance[10]. For initial partonic densities expected at RHIC, the severe violation of Lorentz covariance in the naive cascade algorithm that employs no subdivision artificially reduces elliptic flow and heats up the  $p_\perp$  spectra[8, 11].

We modeled central Au+Au collisions at RHIC with the minijet initial conditions used in Ref. [8]. The evolution started from a longitudinally boost invariant Bjorken tube at proper time  $\tau_0 = 0.1$  fm/c, with locally isotropic momentum distribution and uniform pseudorapidity  $\eta \equiv 1/2 \log[(t+z)/(t-z)]$  distribution between  $|\eta| < 5$  with  $dN_g(\tau_0)/d\eta = 1050$ . The initial transverse density distribution was proportional to the binary collision distribution for two Woods-Saxon distributions, while the  $p_\perp$  distribution was a thermal fit with  $T = 700$  MeV as in Ref. [8].

*Pion freezeout results.* The freezeout distribution  $d^4N/d^4x$  was defined as the distribution of space-time coordinates for the last interaction point of the test particles. Our strong simplifying assumption is that this point is not affected by hadronization. We also neglected resonance contributions to the pion yield. The same  $1g \rightarrow 1\pi$  hadronization model was applied as in Ref. [8] motivated by parton-hadron duality.

Fig. 1 shows the pion freezeout distribution  $d^2N/rdrd\tilde{t}$  (where  $r \equiv \sqrt{x_O^2 + x_S^2}$ ). Three ranges of the average pair transverse momentum are considered. The variation of the distributions with transport opacities  $\chi = 0.60, 3.01$ , and  $7.73$  is shown. For  $dN_g/d\eta = 1050$  these correspond to  $\sigma_{el} = 0.6, 3$ , and  $7.5$  mb. Unlike the sharp freezeout imposed in hydrodynamical models, the transport theory freezeout is a continuous, *evaporation-like* process[10]. For a given (nonzero) opacity, the larger the  $p_\perp$  of the particle, the earlier it decouples and the closer it is to the surface of the nuclei. Low- $p_\perp$  particles freeze out from the center at late times, while high- $p_\perp$  ones escape from the surface early. Furthermore, a larger opacity increases decoupling times, especially for low- $p_\perp$  particles.

Fig. 1 also demonstrates the importance of using a covariant algorithm, such as MPC, for solving Eq. (3). For  $\chi = 7.73$ , the covariant freezeout  $dN/rdrd\tilde{t}$  distribution (third row) differs significantly from that obtained with the naive noncovariant cascade method, i.e., without particle subdivision (fourth row). At the center, the covariant freezeout density decreases with increasing  $p_\perp$ , opposite to the monotonic increase shown by the non-covariant result. Moreover, for the naive algorithm, the freezeout density peaks at the center ( $r \approx 0$ ) for all  $p_\perp$  bins shown, while for the covariant result the maximum moves out towards the surface as  $p_\perp$  increases.

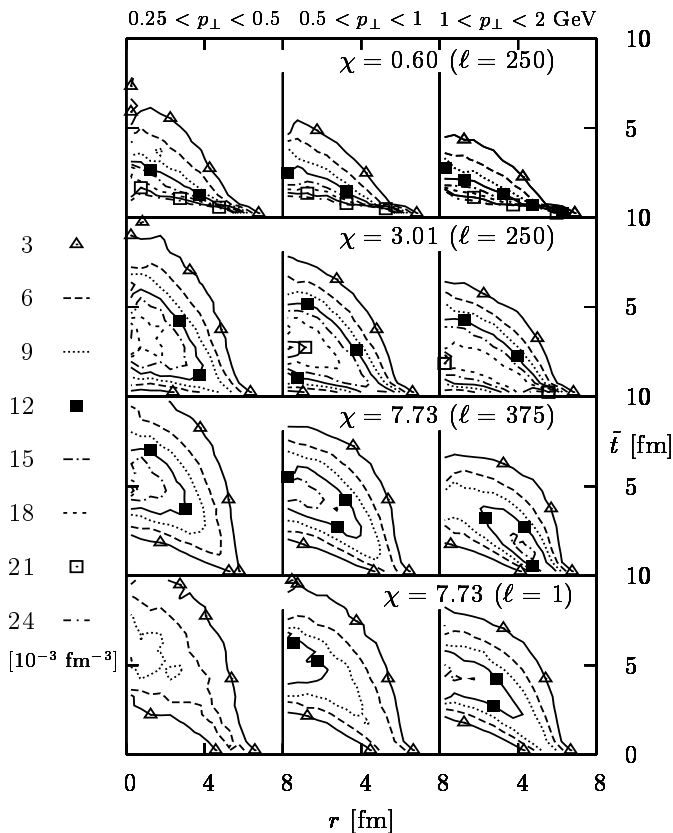


FIG. 1: Contour lines for freezeout distributions  $dN/rdrd\tilde{t}$  from MPC for Au+Au at RHIC as a function of  $p_\perp$  and transport opacity. Distributions are normalized to unity in each  $p_\perp$  bin.

Naturally, Lorentz-violating artifacts also affect the geometric source radii as shown in Fig. 2 for  $\chi = 7.73$ . Compared to the naive cascade algorithm, the covariant one gives smaller  $R_O$  and  $R_L$  for all  $K_\perp$ . The discrepancy is larger for  $R_L$ , and for both radii increases as  $K_\perp$  decreases, leading to about 1 and 2 fm corrections, respectively, at  $K_\perp \approx 0.2$  GeV. It is remarkable that for  $R_S$  the correction changes sign as  $K_\perp$  increases, and that consequently the naive cascade method yields  $R_O/R_S > 1$  for all  $K_\perp$ , while the covariant result shows  $R_O < R_S$  for  $K_\perp > 2$  GeV. In the transport  $R_O < R_S$  occurs because of strong positive dynamical  $x_O - \tilde{t}$  correlations.

Fig. 3 shows a comparison to the HBT radii measured at RHIC. In the transverse opacity range  $\chi \sim 0 - 8$  we studied, the classical transport results are smaller than the observed  $R_O$  and  $R_L$ . This is in sharp contrast to ideal hydrodynamics, which overpredicts both radii[7]. The monotonic dependence of  $R_O$  and  $R_L$  on transport opacity suggests that better agreement with data may be possible with larger opacity  $\chi \sim 20 - 30$ , which unfortunately are numerically impractical as yet. The need for such high opacities is also suggested by the elliptic flow  $v_2(p_\perp)$  saturation analysis[8].

In Fig. 3,  $R_L$  is obviously small for zero opacity because freezeout occurs then at the formation time  $\tau = \tau_0$ . Note

that  $R_L^2 \approx \tau^2 [\Delta(\eta - y)]^2$  depends on the decoupling time and the strength of the  $\eta - y$  correlation. For our thermally correlated initial condition  $[\Delta(\eta - y)]^2 \approx T/m_\perp$  at  $\tau_0 = 0.1$  fm/c.

However, as the transport opacity increases,  $R_L$  grows rapidly because the decoupling time increases as is evident from Fig. 1. The largest increase  $\tau/\tau_0 \sim R/\tau_0 \sim 50$  is for low- $p_\perp$  partons, which freeze out latest. The observed  $R_L(K_\perp)$  is a sensitive probe of the product of the freezeout proper time and  $\Delta(\eta - y)$ . Thus a perfect inside-outside correlation, i.e.,  $\eta = y$ , as assumed in classical Yang-Mills approaches, cannot be reconciled with the RHIC  $R_L$  data, without final state interactions.

In our approach, the main remaining puzzle in Fig. 3 is the predicted  $R_S(K_\perp) \approx const \approx 3$  fm that is peculiarly independent of the transport opacity and underestimates significantly the observed side radius. This suggests that  $R_S$  is insensitive to the early partonic collective dynamics. The same underestimate of  $R_S$  has been found in hydrodynamical calculations as well[7]. The  $R_S$  problem may be related to the assumed longitudinally boost invariant dynamics in both approaches. However, it also could be related to our neglect of hadronic resonances treated in [12, 14]. We also note that for more spherically symmetric initial condition, even ideal hydrodynamical solutions[21] exhibit  $R_O/R_S \sim 1$  with larger side radii.

*Conclusions.* Using the MPC technique, we investigated the effect of early phase dissipative partonic dynamics on the decoupling geometry in heavy-ion collisions in the RHIC energy domain. The pion freezeout distribution at midrapidity was found to be sensitive to the transport opacity of partons as in [14]. The transport freezeout process is similar to evaporation: high- $p_\perp$  particles freeze out early from the surface, while low- $p_\perp$  ones decouple late from the center. For  $K_\perp \lesssim 2$  GeV,  $R_O$  was found to become smaller than  $R_S$  indicating that positive  $x_O - \tilde{t}$  dynamical correlations are strongly sensitive to finite mean free path effects.

We also demonstrated that the naive cascade algorithms without high particle subdivision lead to large numerical artifacts in the freezeout distribution due to violation of Lorentz covariance. These artifacts enhance the out and long radii, especially at low  $K_\perp$ , while increase(reduce)  $R_S$  for  $K_\perp$  below(above)  $\approx 2$  GeV. The MPC technique makes it possible to avoid those artifacts.

While we showed that a decreasing  $R_{out}/R_{side} < 1$  with  $K_\perp$  can arise from covariant parton transport dynamics, the momentum scale where this happens is not realistic due to the simplified local  $g \rightarrow \pi$  hadronization scheme employed as well as the neglect of hadronic transport. A consistent explanation of all the differential features of HBT correlations will have to include in the future a more realistic covariant model of hadronization as well as maintain covariance during the hadronic final state interactions.

*Acknowledgments:* This work is supported by the Director, Office of Science, Office of High Energy and Nuclear Physics, Division of Nuclear Physics, of the U.S.

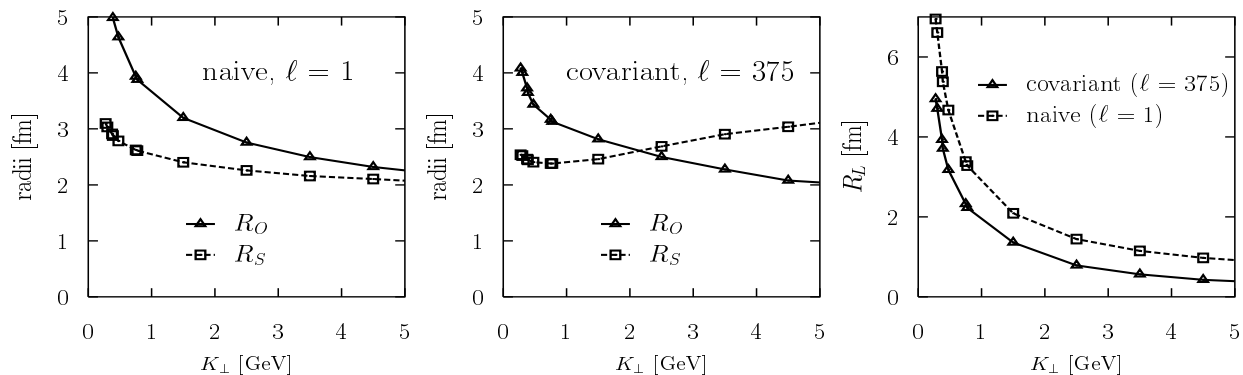


FIG. 2: Strong parton subdivision dependence of the pion HBT radii as a function of  $K_{\perp}$  for transport opacity  $\chi = 7.73$ .

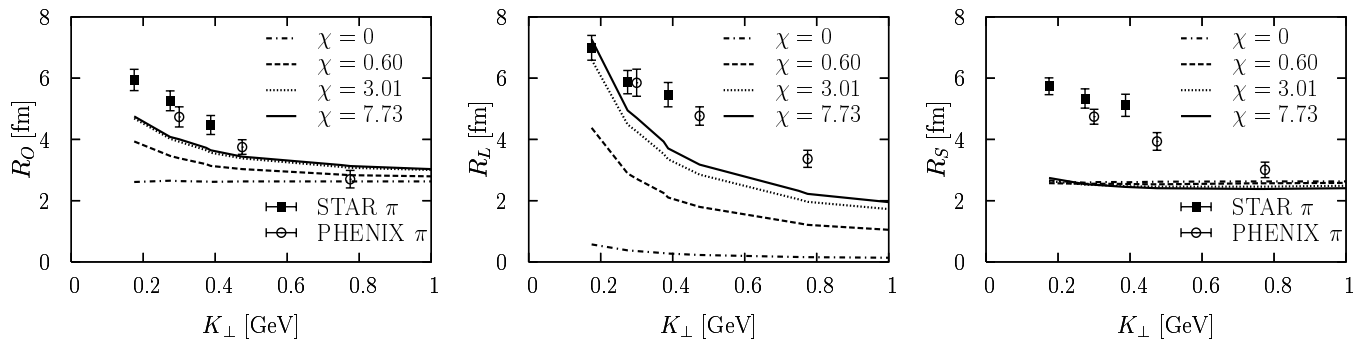


FIG. 3: HBT radii as a function of  $K_{\perp}$  and transport opacity. Data from Refs. [1, 2] are shown.

Department of Energy under Grants No. DE-FG02-93ER40764 and DE-FG02-01ER41190. We acknowledge the Parallel Distributed Systems Facility at the National

Energy Research Scientific Computing Center for providing computing resources.

- 
- [1] C. Adler *et al.* [STAR Collaboration], Phys. Rev. Lett. **87**, 082301 (2001).  
[2] K. Adcox *et al.* [PHENIX Collaboration], Phys. Rev. Lett. **88**, 192302 (2002).  
[3] Preliminary data presented at Quark Matter 2002, showing HBT radii are the same at  $\sqrt{s} = 130$  and 200 AGeV.  
[4] R. J. Snellings [STAR Collaboration], Nucl. Phys. A **698**, 193 (2002); C. Adler *et al.* [STAR Collaboration], nucl-ex/0206006.  
[5] K. Adcox [PHENIX Collaboration], nucl-ex/0204005.  
[6] D. H. Rischke and M. Gyulassy, Nucl. Phys. A **608**, 479 (1996).  
[7] U. W. Heinz and P. F. Kolb, Nucl. Phys. A **702**, 269 (2002); D. Zschesche, H. Stocker, W. Greiner and S. Schramm, Phys. Rev. C **65**, 064902 (2002).  
[8] D. Molnar and M. Gyulassy, Nucl. Phys. A **697**, 495 (2002); Erratum-*ibid* A **703**, 893 (2002).  
[9] B. Zhang, Comput. Phys. Commun. **109**, 193 (1998); Y. Pang, RHIC 96 Summer Study, CU-TP-815 preprint (unpublished).  
[10] D. Molnar and M. Gyulassy, Phys. Rev. C **62**, 054907 (2000).  
[11] S. Cheng, S. Pratt, P. Csizmadia, Y. Nara, D. Molnar, M. Gyulassy, S. E. Vance, and B. Zhang, Phys. Rev. C **65**, 024901 (2002).  
[12] S. Soff, S. A. Bass and A. Dumitru, Phys. Rev. Lett. **86**, 3981 (2001); S. Soff, S. A. Bass, D. H. Hardtke and S. Y. Panitkin, nucl-th/0209055.  
[13] T. J. Humanic, nucl-th/0205053.  
[14] Z. W. Lin, C. M. Ko and S. Pal, Phys. Rev. Lett. **89**, 152301 (2002).  
[15] T. Csorgo and A. Ster, nucl-th/0207016.  
[16] D. Molnar and M. Gyulassy, nucl-th/0204062, Heavy Ion Phys. in press.  
[17] D. Molnár, MPC 1.6.0. This transport code used in the letter can be downloaded from WWW at <http://www-cunuke.phys.columbia.edu/people/molnard>.  
[18] M. Gyulassy, S. K. Kauffmann and L. W. Wilson, Phys. Rev. C **20**, 2267 (1979).  
[19] T. Csorgo, hep-ph/0001233.  
[20] U. A. Wiedemann and U. W. Heinz, Phys. Rept. **319**, 145 (1999).  
[21] M. Gyulassy and D. Rischke, [http://bp2002.kfki.hu/Proc/Gyulassy/gyul\\_bp02.ps.gz](http://bp2002.kfki.hu/Proc/Gyulassy/gyul_bp02.ps.gz), Heavy Ion Phys. in press.